Microchimica Acta (2020) 187:652
https://doi.org/10.1007/s00604-020-04629-5

ORIGINAL PAPER

Photothermal and fluorescent dual-mode assay based on the formation of polydopamine nanoparticles for accurate determination of organophosphate pesticides

Xiaofeng Liu[1] · Zhaoxing Wu[1] · Xiaohai Yang[1] · Qing Wang[1] · Liyuan Zou[1] · Wenjing Mei[1] · Yan Zheng[1] · Kemin Wang[1]

Received: 7 August 2020 / Accepted: 28 October 2020

Abstract

A photothermal and fluorescent dual-mode assay for sensitive organophosphate pesticides (Ops) determination is reported based on alkaline phosphatase (ALP)-inhibition-induced formation of polydopamine (PDA) nanoparticles. In the presence of ALP, ascorbic acid 2-phosphate (AAP) can be catalyzed to produce ascorbic acid (AA). AA can reduce MnO_2 nanosheets, further inhibiting the oxidation of dopamine (DA). Ops as an inhibitor for ALP activity prevents the formation of AA and the reduction of MnO_2 nanosheets. Eventually, the formation of PDA nanoparticles is promoted. The inhibitory effect of Ops on ALP activity causes obvious changes of photothermal signals and fluorescence signal at 495 nm. The detection limit (LOD) of dimethoate is 0.1 μM. The method displays excellent sensing capability for the dimethoate assay in real water with good recoveries of 99.4–107.6%.

Keywords Dual-signal assay · Dimethoate · Alkaline phosphatase · Polydopamine

Introduction

Organophosphate pesticides (Ops) are widely applied substances in modern agricultural activities and play important role in ensuring food production [1–3]. However, Ops contamination resulting from excessive use has become one of the most arduous environmental protection challenges [4, 5]. Specifically, Ops work as a toxicity on central nervous system of human by inactivating acetylcholinesterase (AChE) at very low concentration, which might cause injure to human body even death [6, 7]. For reducing Ops poisoning, accurate determination of trace Op is essential and significant.

Many quantitative methods have been employed to determine Ops. The most commonly used methods include nuclear magnetic resonance spectrum (NMR), chromatography, and gas chromatography coupled with mass spectrometry (GC/MS) [4, 8–10]. These detection methods are accurate; however, most have some weaknesses, such as high cost and dependence on professional technology or advanced instruments, which restricts their applications. Recently, some convenient and low-cost methods have been developed for Ops determination [11–14]. But most of them are single readout assays. These single-mode methods only provide limited information and are susceptible to external interference, which may cause false signals, while the dual-mode method increases the diversity of information. Besides, the output results of dual-mode method can be mutually verified, which significantly improve the accuracy and reliability of the results [15–19]. To our knowledge, the application of dual-mode strategy to determine Ops has so far been relatively rare. For example, Su et al. designed a fluorometric and colorimetric dual-mode sensor for sensitive paraoxon assay based on fluorescence quenching of carbon dots (CDs) trigged by AChE [20]. Lu et al. developed an electrochemical and colorimetric dual-

Xiaofeng Liu and Zhaoxing Wu contributed equally to this work.

Supplementary Information The online version contains supplementary material available at https://doi.org/10.1007/s00604-020-04629-5.

✉ Qing Wang
wwqq99@hnu.edu.cn

✉ Kemin Wang
kmwang@hnu.edu.cn

[1] State Key Laboratory of Chemo/Biosensing and Chemometrics, College of Chemistry and Chemical Engineering, Key Laboratory for Bio-Nanotechnology and Molecular Engineering of Hunan Province, Hunan University, Changsha 410082, China

Published online: 11 November 2020

readout lab-on-paper platform for paraoxon's on-site monitoring [21]. Thus, it is necessary to develop dual-mode approach for Ops determination.

In our previous work, a portable photothermal assay based on the polydopamine (PDA) nanoparticles for point-of-care (POC) determination of alkaline phosphatase (ALP) enzyme was developed [22]. However, the result of photothermal sensor is susceptible to ambient environment, including air temperature. To prevent false signal, it is a promising strategy to integrate photothermal sensing with other assay methods. Recently, the adaptation of fluorescence properties of PDA to the biochemical analysis has received great research interest resulting from the excellent sensitivity and convenience [23, 24]. In this study, a dual-mode assay for accurate determination of Ops utilizing the photothermal and fluorescent properties of PDA nanoparticles was developed. As illustrated in Scheme 1, MnO_2 can oxidize dopamine into dopamine-quinone, then undergoes intramolecular cyclization, oxidization, and rearrangement, and eventually self-assembles to form PDA nanoparticles which possess photothermal and fluorescent signals [25, 26]. ALP enzyme can catalyze the dephosphorylation of ascorbic acid 2-phosphate (AAP) and yield ascorbic acid (AA). Then, MnO_2 nanosheet is deoxygenized by AA and generated Mn^{2+}, accompanied by the formation of dehydrogenated ascorbic acid (DHA), eventually inhibiting the formation of PDA nanoparticles. However, Ops working as an inhibitor of ALP prevent the yield of AA and decomposition of MnO_2 nanosheets, resulting in the generation of PDA nanoparticles with oxidation of MnO_2 nanosheets. The Ops concentration in solution directly influences ALP activity, which ultimately determined the photothermal and fluorescent signal changes. The designed method can be accomplished without the help of any heavy or expensive instrumentation, which is meaningful for on-site determination of Ops.

Experimental section

Preparation and characterization of MnO_2 nanosheets and polydopamine nanoparticles

MnO_2 nanosheets were synthesized employed a redox method [22] (shown in Electronic Supporting Material (ESM) in detail). The synthesized MnO_2 nanosheets were characterized by JEM-2100Plus (JEOL, Japan) and UV-2600 spectrophotometer (Shimadzu, Japan).

An existing synthesis method was adopted to synthesize PDA nanoparticles [26, 27] (shown in ESM in detail). The synthesized PDA nanoparticles were characterized by JEM-2100Plus (JEOL, Japan) and F-7000 (Hitachi, Japan).

Organophosphate pesticides determination

Dimethoate was selected as a model analyte to explore the inhibition effect on ALP activity to induce formation of PDA nanoparticles. Different consistencies of dimethoate with final concentrations of 0–2000 μM were incubated with 100 U L^{-1} ALP, 23 μg mL^{-1} AAP, and 20 μg mL^{-1} MnO_2 in pH 7.4 Tris-HCl buffer at 30 °C for 40 min. Next, dopamine solution (20 μg mL^{-1}) was mixed with the reaction solution. After stirring, the solution was kept on incubation at 25 °C for 0.5 h. Finally, 20 μL HCl solution (0.1 M) was added into the solution to stop the reaction. For photothermal assay, the resulting solution was irradiated with 780-nm laser for 10 min. A thermometer was applied to measure the photothermal signal of resulting solution. For fluorescent assay, the resulting solution used was measured F-7000 (Hitachi, Japan) (the main parameters: both excitation and emission slit width are 5 nm; voltage is 950 V; excitation wavelength is 495 nm; and emission wavelength is 400 nm).

Real water was gathered from Xiang River in Changsha, China. The water samples were firstly filtered three times and

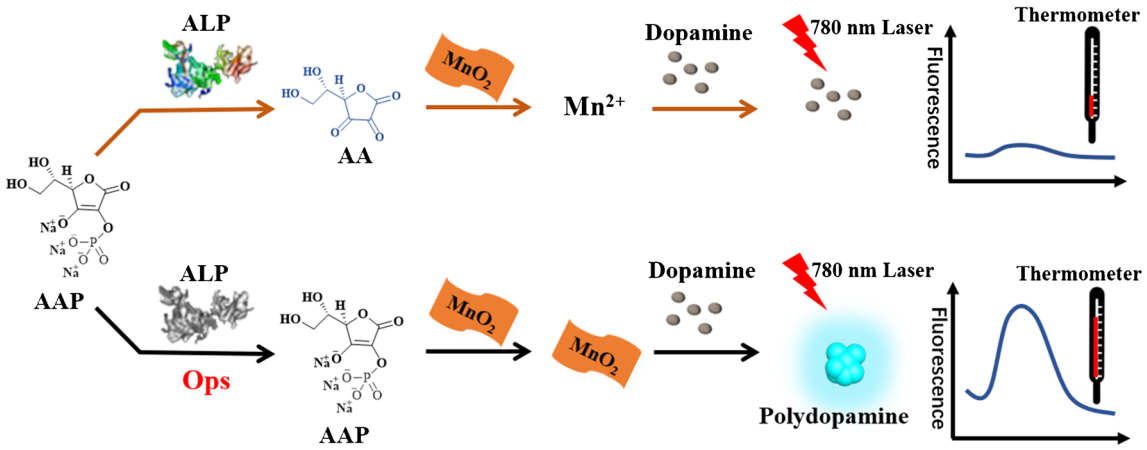

Scheme 1 Schematic illustration of photothermal and fluorescent dual-mode assay for Ops determination

the pretreat water samples were regarded as buffer for subsequent experiment. Next, dimethoate with different concentrations was mixed with river water to yield solutions with final dimethoate concentrations of 0–2000 μM. The above solutions were analyzed using the proposed dual-mode method. In addition, different quantities of dimethoate were directly added to tap water samples to produce solutions with final omethoate concentrations of 1, 10, 50, and 100 μM. The spiked samples were analyzed and the concentration of dimethoate was estimated according to the regression equation. Then, the recovery rates of tap water samples spiked with dimethoate were calculated. To verify universal applicability of the biosensor, the assay (not added dimethoate in real samples) was chosen as a contrast.

Results and discussion

Characterization of MnO_2 nanosheets

A one-pot method was applied to synthesize MnO_2 nanosheets. In contrast to the previous methods [28–30], the proposed method possesses some advantages including reducing the time required for synthesis and avoiding harsh experimental conditions (such as high pressure). The synthesized MnO_2 nanosheets were characterized utilized some techniques. TEM image in Fig. S1A clearly shows a clear two-dimensional sheet-like shape of the synthesized MnO_2 nanosheets. EDS spectrum proves the appearance of oxygen (O) elements and manganese (Mn), with an atomic ratio of 2:1 (Fig. S1B). The UV-vis spectrum of the MnO_2 nanosheets shows a distinct absorption peak at 400 nm, in accordance with previous reports (Fig. S1C) [31]. Besides, MnO_2 nanosheets have good dispersibility in aqueous solution and can remain dispersed for 3 weeks without agglomeration.

Characterization of polydopamine nanoparticles

PDA nanoparticles were produced through MnO_2 nanosheets oxidizing dopamine. The morphology of PDA nanoparticles was characterized by TEM. The image (Fig. 1a) illustrates that the nanoparticles are almost spherical in shape and show excellent dispersion in water. Besides, the insert histogram presents the size distribution of the PDA nanoparticles that ranges in diameter from about 6 to 12 nm, and the peak position is determined to be 9 nm. PDA nanoparticles show identically well-resolved lattice fringes with interplanar spacings of 0.21 nm (Fig. 1b). Besides, EDS

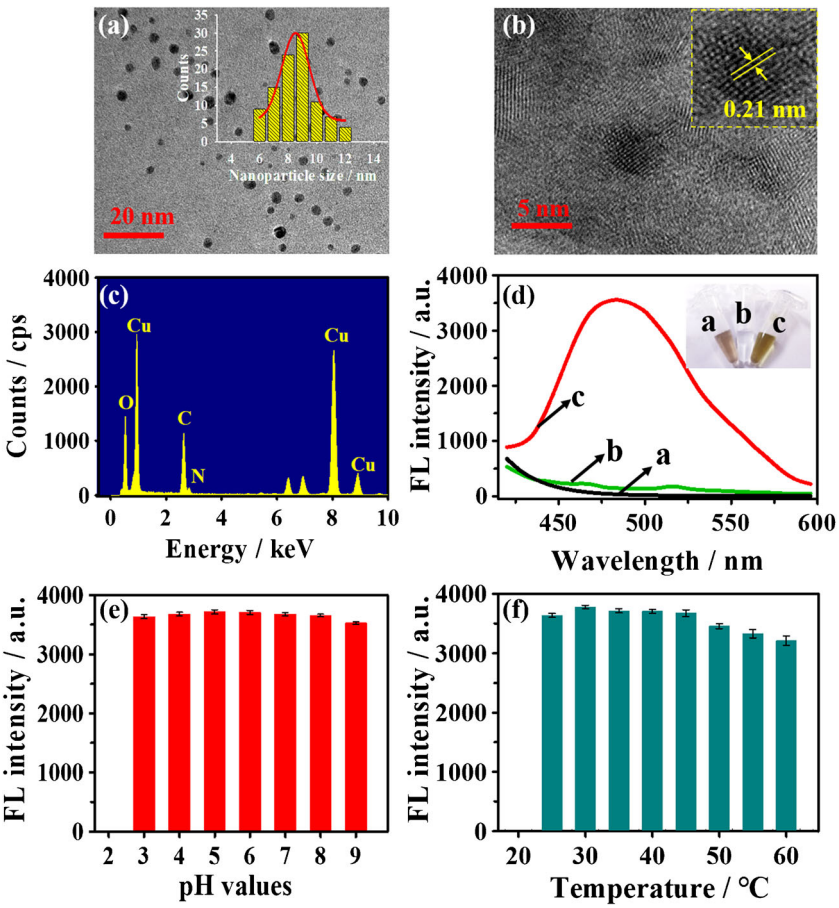

Fig. 1 The morphology and fluorescent characterization of PDA nanoparticles. **a** TEM observation of the synthesized PDA nanoparticles. Scale bar, 20 nm (insert: histogram of particle size (diameter) distribution of PDA nanoparticles). **b** High-resolution TEM graphics (scale bar, 5 nm) and **c** EDS spectrum of PDA nanoparticles. **d** Fluorescence spectra of (a) MnO_2, (b) dopamine, and (c) dopamine + MnO_2. Changes in fluorescence intensity of the PDA nanomaterials at 495 nm with distinct pH (**e**) and temperature (**f**). Error bars are standard deviation of three repetitive experiments

spectrum of the PDA nanoparticles demonstrates the appearance of carbon (C), nitrogen (N), and oxygen (O) elements (Fig. 1c). Copper peak in Fig. 1c originates from the TEM supporting carbon-coated copper grid. While no manganese (Mn) element is observed. It implies that PDA and MnO_2 do not form a core-shell-structure nanocomposite, which is consistent with the previous work [26].

Next, the fluorescence properties of PDA nanoparticles were characterized. As shown in Fig. 1d, neither dopamine nor MnO_2 has clear fluorescence unless they are mixed. The obtained fluorescent PDA nanoparticles show the maximum emission intensity at 495 nm. In Fig. 1e, the fluorescent intensity does not change obviously as the pH value of the solution rose from 3.0 to 9.0. Besides, the results (Fig. 1f) illustrate the fluorescent intensity of PDA nanoparticles keeps stable when the ambient temperature raises from 25 to 60 °C. These consequences confirm that the PDA nanoparticles have superior fluorescence stability.

Besides, the photothermal properties of PDA nanoparticles were also characterized. The temperature of the mixture solution of dopamine and MnO_2 rises gradually after 20 min laser irradiation, while an ignorable temperature change occurred in the MnO_2 nanosheets or dopamine solution shown in Fig. S2A. The data demonstrates that the PDA nanoparticles possess superior photothermal effect, in keeping with the previous works [22]. Another experiment is also taken to test the photostability of PDA nanoparticles. As shown in Fig. S2B, obvious photobleaching is not observed after PDA nanoparticles undergo 5 cycle irradiations. These results demonstrate the PDA nanoparticles have outstanding photothermal stability.

Dual-mode determination of organophosphate pesticides in buffer

The photothermal and fluorescent response under different parameters (including buffer, the ratio of MnO_2 nanosheets and DA, the reaction time, and AAP concentration) was explored simultaneously. As shown in Fig. S3, 10 mM Tris-HCl (pH 7.4) buffer, 1:1.4 of concentration ratio of MnO_2 nanosheets and DA, 40 min of reaction time, and 23 mM AAP concentration are chosen in the following experiment.

To test the applicability of the established dual-mode assay, the inhibition efficiency of the sensing system with different concentrations of dimethoate was measured. As shown in Fig. 2a, the thermal response of PDA nanoparticles after the irradiation progressively rises in pace with the increasing of dimethoate concentration value. Figure 2b shows the change trend of temperature signal change ($\Delta T - \Delta T_0$) with various concentrations of dimethoate. The inset of Fig. 2b illustrates that the temperature signal change is proportional to the logarithm of dimethoate concentrations of 1 to 2000.0 μM. The

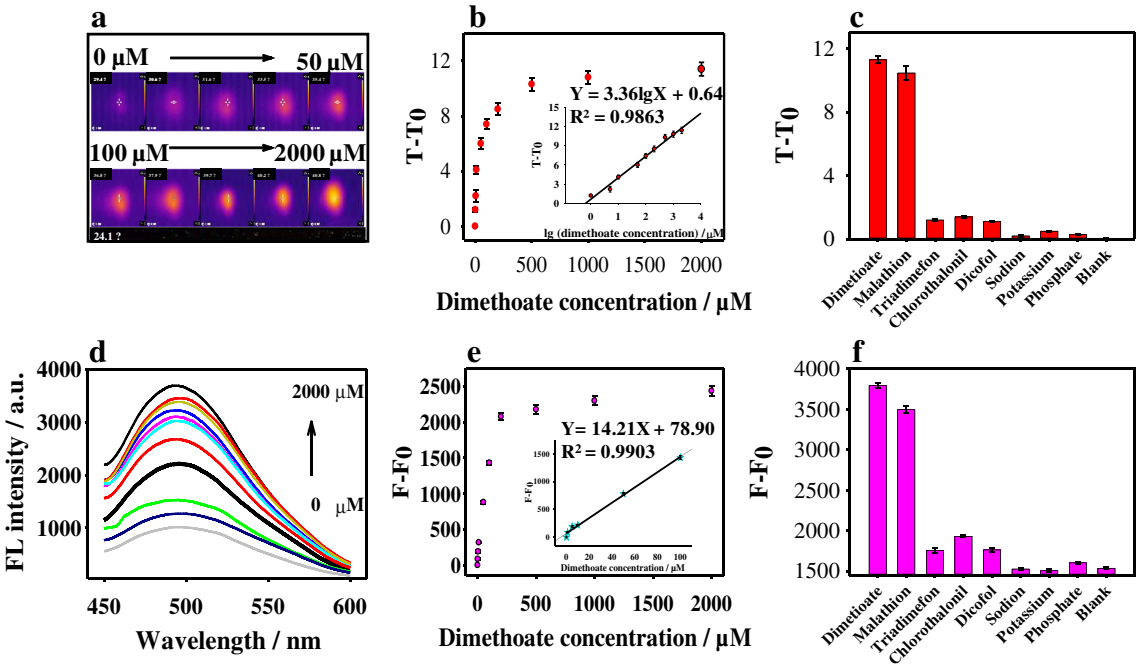

Fig. 2 Sensitivity and selectivity investigation of the proposed assay. **a** The thermal response after irradiation (780 nm, 10 min) for target dimethoate at concentrations of 0, 1, 5, 10, 50, 100, 200, 500, 1000, and 2000 μM. **b** Correlation between temperature change values ($T - T_0$) and the concentration of dimethoate (0.0 to 2000.0 μM). **c** The selective investigation of the fluorescence mode. **d** Fluorescence spectra of PDA with different concentrations of dimethoate (both excitation and emission slit width are 5 nm; voltage is 950 V; excitation wavelength is 495 nm; and emission wavelength is 400 nm). **e** Correlation between fluorescence intensity change values ($F - F_0$) and the dimethoate concentration (0.0 to 2000.0 μM). **f** The selective investigation of the photothermal mode. Error bars are the standard deviation of three repetitive experiments

regression equation is $Y = 3.36 \times \lg X + 0.64$ with a correlation coefficient R^2 of 0.9863. Y is temperature signal change ($\Delta T - \Delta T_0$). X is the dimethoate concentration. ΔT_0 is the temperature signal change after irradiation without dimethoate. ΔT is the temperature signal change after irradiation when dimethoate appears. The detection of limit (LOD) of dimethoate is estimated to be 0.1 μM ($S/N = 3$).

Afterward, the performance of fluorescent sensing is also explored with the increase of dimethoate concentration. The fluorescence intensity at 495 nm gradually rises along with the increasing of dimethoate concentration (0.0 to 2000.0 μM) (Fig. 2d). As Fig. 2d shows, the increase of concentrations of dimethoate results in strengthening of the fluorescence intensity. The inset of Fig. 2e illustrates the fluorescence intensity changes linearly against the concentration of dimethoate (1 to 100 μM). The regression equation is $Y = 14.21X + 78.90$ ($R^2 = 0.9903$). Y is fluorescence intensity. X is defined as the dimethoate concentration. The LOD of dimethoate is estimated to be 0.1 μM ($S/N = 3$). It is lower than the standard limit of dimethoate residue in centralized surface water source for drinking water (0.3 μM) defined by the Ministry of Ecology and Environment of China [32]. It implies that the strategy may meet actual requirements. As shown in Table S1, compared with other methods for Ops or dimethoate determination, the dual-mode method has a wide detection range and low detection limit. Besides, the method which integrated the photothermal and fluorescent mode can reduce the possibility of false signals as much as possible, so it has superior accuracy and reliability.

Specificity is another significant characteristic to evaluate the performance of sensing platform. The signal changes of the platform towards common pesticides, such as triazoles (triadimefon), organochlorine (chlorothalonil and dicofol), Ops (malathion), sodium, potassium, and phosphate, were investigated. The histogram (Fig. 2c, f) reveal that triadimefon, chlorothalonil, dicofol, sodium, potassium, and phosphate generate weak fluorescence and temperature signal compared to blank sample. However, Ops including dimethoate and malathion cause remarkable positive response. It demonstrates that these interference substances have slight effect on the sensing platform, suggesting that the assay has excellent selectivity towards Ops. In theory, other reducing substances such as glutathione may affect the sensing performance by reducing MnO_2. However, the concentration of glutathione in real water is too low to affect the sensing performance. The standard limits of other small reducing molecules residue including formaldehyde, acetaldehyde, aniline, benzidine, and hydrazine hydrate in centralized surface water source for drinking water are also very low [32]. Therefore, these reducing molecules can cause ignorable effect on the sensing performance.

Organophosphate pesticides determination in real water

To assess the reliability of the method in real samples, the dimethoate in river water was determined using the designed PDA-nanoparticles-based photothermal and fluorescent dual-mode assay. As shown in Fig. S4A and Fig. S4B, whether in river water samples or in buffer, the photothermal and fluorescent signal changes against the target dimethoate concentration are basically consistent. As shown in Table 1, the recovery rates for four spiked dimethoate concentrations (1, 10, 50, 100 μM) in tap water are in an accurate range of 99.4–107.6%. The dual-mode method exhibits good accuracy with a relative standard deviation (RSD) less than 4.99%, which confirms that the proposed dual-mode method matches the requirement of dimethoate determination in real water. The above results suggest that the dual-mode platform has potential worth for dimethoate determination in practical samples.

Conclusions

In conclusion, a dual-mode assay was designed for quantification of Ops based on ALP-inhibition-induced formation of PDA nanoparticles. Given that PDA nanoparticles possess excellent photothermal and fluorescent properties, this assay integrated dual-mode can reduce the possibility of false signals for ensuring reliability. Besides, the assay can be completed without the assistance of any heavy or costly instrumentation, which is meaningful for on-site determination of Ops. The method possesses superior sensing capability for Ops analysis in practical samples. However, the proposed method is time-consuming and cannot be regenerated, which might limit the POC application. In the future, we will further improve the experimental conditions to achieve rapid POC determination of Ops.

Table 1 Results of the determination of dimethoate in spiked real samples

	Fluorescent method				Photothermal method		
Sample	Spiked (μM)	Found (μM)	Recovery (%)	RSD ($n = 3$, %)	Found (μM)	Recovery (%)	RSD ($n = 3$, %)
Tap water	1	1.02	102	0.27	1.07	107	0.47
	10	10.76	107.6	1.13	10.24	102.4	1.10
	50	50.11	100.2	1.48	49.70	99.4	4.30
	100	99.65	99.6	4.99	100.43	100.4	3.21

Acknowledgments This work was carried out within the framework of the National Natural Science Foundation of China (Grants 22074032, 21675047, and 21735002) and National Science Foundation for Distinguished Young Scholars of Hunan Province (2016JJ1008).

Compliance with ethical standards

Conflict of interest The authors declare that they have no competing interests.

References

1. Pundir CS, Malik A, Preety (2019) Bio-sensing of organophosphorus pesticides: a review. Biosens Bioelectron 140:5–17
2. Jin R, Kong D, Yan X, Zhao X, Li H, Liu F, Sun P, Lin Y, Lu G (2019) Integrating target-responsive hydrogels with smartphone for on-site ppb-level quantitation of organophosphate pesticides. ACS Appl Mater Interfaces 11:27605–27614
3. Tang J, Li J, Xiong P, Sun Y, Zeng Z, Tian X, Tang D (2020) Rolling circle amplification promoted magneto-controlled photoelectrochemical biosensor for organophosphorus pesticides based on dissolution of core-shell MnO_2 nanoflower@CdS mediated by butyrylcholinesterase. Microchim Acta 187:450
4. Liu M, Khan A, Wang Z, Liu Y, Yang G, Deng Y, He N (2019) Aptasensors for pesticide detection. Biosens Bioelectron 130:174–184
5. Yan X, Li H, Su X (2018) Review of optical sensors for pesticides. TrAC Trends in Anal Chem 103:1–20
6. Arduini F, Cinti S, Caratelli V, Amendola L, Palleschi G, Moscone D (2019) Origami multiple paper-based electrochemical biosensors for pesticide detection. Biosens Bioelectron 126:346–354
7. Yang M, Liu M, Wu Z, He Y, Ge Y, Song G, Zhou J (2019) Carbon dots co-doped with nitrogen and chlorine for "off-on" fluorometric determination of the activity of acetylcholinesterase and for quantification of organophosphate pesticides. Microchim Acta 186:585
8. Bucur B, Munteanu FD, Marty JL, Vasilescu A (2018) Advances in enzyme-based biosensors for pesticide detection. Biosensors 8:7–55
9. Wang X, Jia R, Song Y, Wang M, Zhao Q, Sun S (2019) Determination of pesticides and their degradation products in water samples by solid-phase extraction coupled with liquid chromatography-mass spectrometry. Microchem J 149:104013
10. Zarejousheghani M, Walte A, Borsdorf H (2018) Sprayed liquid-gas extraction of semi-volatile organophosphate malathion from air and contaminated surfaces. Anal Methods 10:2503–2511
11. Liu Y, Lin X, Ji X, Hao Z, Tao Z (2020) Smartphone-based enzyme-free fluorescence sensing of organophosphate DDVP. Microchim Acta 187:419
12. Cheng N, Shi Q, Zhu C, Li S, Lin Y, Du D (2019) Pt-Ni$(OH)_2$ nanosheets amplified two-way lateral flow immunoassays with smartphone readout for quantification of pesticides. Biosens Bioelectron 142:111498
13. Yan X, Song Y, Zhu C, Li H, Du D, Su X, Lin Y (2018) MnO_2 nanosheet-carbon dots sensing platform for sensitive detection of organophosphorus pesticides. Anal Chem 90:2618–2624
14. Song Y, Yan X, Li Z, Qu L, Zhu C, Ye R, Li S, Du D, Lin Y (2018) Highly photoluminescent carbon dots derived from linseed and their applications in cellular imaging and sensing. J Mater Chem B 6:3181–3187
15. Liu D, Chen W, Wei J, Li X, Wang Z, Jiang X (2012) A highly sensitive, dual-readout assay based on gold nanoparticles for organophosphorus and carbamate pesticides. Anal Chem 84:4185–4191
16. Wei Y, Wang D, Zhang Y, Sui J, Xu Z (2019) Multicolor and photothermal dual-readout biosensor for visual detection of prostate specific antigen. Biosens Bioelectron 140:48–56
17. Lu HF, Zhang MM, Wu D, Huang JL, Zhu LL, Wang CM, Zhang QL (2018) Colorimetric and fluorescent dual-mode sensing of alkaline phosphatase activity in L-02 cells and its application in living cell imaging based on in-situ growth of silver nanoparticles on graphene quantum dots. Sens Actuators B Chem 258:461–469
18. Ye S, Wu Y, Wan F, Li Y (2019) A seesaw ratiometric probe for dual-spectrum imaging and detection of telomerase activity in single living cells. Chem Commun 55:9967–9970
19. Cao H, Wang Y, Gao Y, Deng X, Cong Y, Liu Y, Jiang X (2019) Molecular design of beta-sheet peptide for the multi-modal analysis of disease. Angew Chem Int Ed 58:1626–1631
20. Li H, Yan X, Lu G, Su X (2018) Carbon dot-based bioplatform for dual colorimetric and fluorometric sensing of organophosphate pesticides. Sens Actuators B Chem 260:563–570
21. Jin R, Kong D, Zhao X, Li H, Yan X, Liu F, Sun P, Du D, Lin Y, Lu G (2019) Tandem catalysis driven by enzymes directed hybrid nanoflowers for on-site ultrasensitive detection of organophosphorus pesticide. Biosens Bioelectron 141:111473
22. Liu X, Zou L, Yang X, Wang Q, Zheng Y, Geng X, Liao G, Nie W, Wang K (2019) Point-of-care assay of alkaline phosphatase enzymatic activity using a thermometer or temperature discoloration sticker as readout. Anal Chem 91:7943–7949
23. Lin ZY, Xue SF, Chen ZH, Han XY, Shi G, Zhang M (2018) Bioinspired copolymers based nose/tongue-mimic chemosensor for label-free fluorescent pattern discrimination of metal ions in biofluids. Anal Chem 90:8248–8253
24. Yildirim A, Bayindir M (2014) Turn-on fluorescent dopamine sensing based on in situ formation of visible light emitting polydopamine nanoparticles. Anal Chem 86:5508–5512
25. Liu Y, Ai K, Lu L (2014) Polydopamine and its derivative materials: synthesis and promising applications in energy, environmental, and biomedical fields. Chem Rev 114:5057–5115
26. Kong XJ, Wu S, Chen TT, Yu RQ, Chu X (2016) MnO_2-induced synthesis of fluorescent polydopamine nanoparticles for reduced glutathione sensing in human whole blood. Nanoscale 8:15604–15610
27. Xiao T, Sun J, Zhao J, Wang S, Liu G, Yang X (2018) FRET effect between fluorescent polydopamine nanoparticles and MnO_2 nanosheets and its application for sensitive sensing of alkaline phosphatase. ACS Appl Mater Interfaces 10:6560–6569
28. Zhu J, He J (2012) Facile synthesis of graphene-wrapped honeycomb MnO_2 nanospheres and their application in supercapacitors. ACS Appl Mater Interfaces 4:1770–1776
29. Deng R, Xie X, Vendrell M, Chang YT, Liu X (2011) Intracellular glutathione detection using MnO_2 nanosheet-modified upconversion nanoparticles. J Am Chem Soc 133:20168–20171
30. He D, He X, Wang K, Yang X, Yang X, Li X, Zou Z (2014) Nanometer-sized manganese oxide-quenched fluorescent oligonucleotides: an effective sensing platform for probing biomolecular interactions. Chem Commun 50:11049–11052
31. Ou M, Huang J, Yang X, Quan K, Yang Y, Xie N, Wang K (2017) MnO_2 nanosheet mediated "DD-A" FRET binary probes for sensitive detection of intracellular mRNA. Chem Sci 8:668–673
32. National Standards of the People's Republic of China, GB 3838–2002, Environmental Quality Standards for Surface Water. State Environmental Protection Agency (SEPA)